Ferromagnetism in Mn-implanted epitaxially grown Ge on Si(100)

S. Guchhait, M. Jamil, H. Ohldag, A. Mehta, E. Arenholz, G. Lian, A. LiFatou, D. A. Ferrer, J. T. Markert, L. Colombo, and S. K. Banerjee

Phys. Rev. B **84**, 024432 — Published 29 July 2011

DOI: 10.1103/PhysRevB.84.024432

FERROMAGNETISM IN MN-IMPLANTED EPITAXIALLY GROWN GE ON SI (100)

S. Guchhait[1*], M. Jamil[1], H. Ohldag[2], A. Mehta[2], E. Arenholz[3], G. Lian[4],
A. LiFatou[4], D. A. Ferrer[1], J. T. Markert[5], L. Colombo[4] and S. K. Banerjee[1†]

[1]Microelectronics Research Center, The University of Texas at Austin, Austin, TX
[2]Stanford Synchrotron Radiation Lightsource, Menlo Park, CA
[3]Advanced Light Source, Berkeley, CA
[4]Texas Instruments Incorporated, Dallas, TX
[5]Department of Physics, The University of Texas at Austin, Austin, TX

ABSTRACT

We have studied ferromagnetism of Mn-implanted epitaxial Ge films on silicon. The Ge films were grown by ultra high vacuum chemical vapor deposition using a mixture of germane (GeH_4) and methylgermane (CH_3GeH_3) gases with a carbon concentration less than 1at%, and observed surface rms roughness of about 0.5 nm, as measured by atomic force microscopy. Manganese ions were implanted in epitaxial Ge films grown on Si (100) wafers to an effective concentration of about 16at%, 12at%, 6at% and 2at%. SQUID measurements showed that only the three highest Mn concentration samples are ferromagnetic, while the fourth sample, with [Mn]=2at%, is paramagnetic. X-ray absorption spectroscopy (XAS) and X-ray Magnetic Circular Dichroism (XMCD) measurements indicate that localized Mn moments are ferromagnetically coupled below the Curie temperature. Isothermal annealing of Mn-implanted Ge films with [Mn]=16at% at 300^{o}C for up to 1200 seconds decreases the magnetization but does not change the Curie temperature, suggesting that the amount of the magnetic phase slowly decreases with time at this anneal temperature. Furthermore, transmission electron microscopy (TEM) and synchrotron grazing incidence x-ray diffraction (GI-XRD) experiments show that the Mn-implanted region is amorphous, and we believe that it is this phase that is responsible for the ferromagnetism. This is supported by our observation that high temperature annealing leads to recrystallization and transformation of the material into a paramagnetic phase.

* samaresh@physics.utexas.edu
† banerjee@ece.utexas.edu

Keywords: Manganese, ion-implant, epitaxial Ge, ferromagnetism, hysteresis, XMCD, XAS, annealing, recrystallization, grazing-incident X-ray diffraction, SIMS, Tunneling Electron Microscopy, XPS, SQUID.

I. INTRODUCTION

Over the last two decades, pioneering research has been performed on dilute magnetic semiconductors (DMS). As a result we now have two systems of transition metal doped III-V based dilute magnetic semiconductors, (Ga,Mn)As and (In,Mn)As. The origin of magnetism in these materials is now fairly well understood as carrier-mediated ferromagnetism [1]. Because of the development of these new materials, many groups have been investigating their use for spintronic devices.

Epitaxial (Ga,Mn)As layers grown by molecular beam epitaxy (MBE) have shown ferromagnetism for Mn concentrations as low as 1% to about 12%. The Curie temperature of this material system is found to be a linear function of the effective Mn concentration from as low as about 10 K to about 180 K [1]. Structural analysis of (Ga,Mn)As shows that the Mn ions can occupy two sites within the GaAs lattice. The majority of Mn atoms substitute Ga sites and other Mn atoms are at interstitial sites. The Mn_{Ga} atoms have a total angular momentum of S=5/2 and act as shallow acceptors. The Mn atoms at interstitial sites on the other hand act as double donors. Ferromagnetism is observed when the impurity band merges with the valence band as then these impurity states become delocalized. At this Mn concentration level, the interaction between local Mn atoms is mediated by the holes in the valence band. Since this magnetic interaction is carrier mediated, it can be controlled by a number of different techniques such as gate voltage, doping, photo-excitation, and band structure engineering. It is this property that opens up the possibilities for many new technologies, including spintronics, current-induced magnetization reversal, quantum computation, etc [1].

The main challenge with dilute magnetic semiconductor material thin films, including (III,Mn)V today, is that the Curie temperature is still well below room temperature. There is significant effort in trying to develop new DMS materials with a Curie temperature higher than room temperature. One promising material system is Mn-doped Ge because of its compatibility with Si processing. Theoretical studies show that Mn dopants will prefer to occupy substitutional sites in a crystalline Ge lattice [2] and one can optimize Mn doping by adding other codopants [3,4]. Theoretical modeling also predicts enhanced magnetic properties and higher solubility of

Mn-doped amorphous Si and Ge systems [5]. There have been a number of reports on experimental studies of ferromagnetism of Mn-doped Ge systems [6-18], with some groups reporting Curie temperatures near room temperature for nanowires [19,20] and above room temperature for nanocolumns [21] and quantum dots [22]. Three different growth techniques have been employed to produce epitaxial Mn-doped Ge films: low temperature MBE [6-10], ultrahigh vacuum thermal coevaporation [11], and high energy Mn-ion implantation into single crystal Ge [12-15]. High temperature furnace melting techniques have also been used to produce bulk Mn-doped Ge samples [16-18]. Besides all of these methods, chemical synthesis techniques have been used to grow $Ge_{1-x}Mn_x$ nanowires [19,20] and MBE has been used to grow Mn-rich nanocolumns [21] and quantum dots [22] embedded in Mn-poor matrix. The nanowire, nanocolumn and quantum dot results suggest that there could be a possibility of developing Mn-doped Ge epitaxial films with Curie temperatures above room temperature. However, so far there are no reports on room temperature gate-bias controlled ferromagnetic material for continuous thin films.

A major problem in all these epitaxial and bulk $Ge_{1-x}Mn_x$ studies is the presence of different phases in those samples. For example, Sugahara *et al*. [9] have shown the presence of a Mn-rich amorphous phase in MBE grown crystalline epitaxial films and they also have claimed that the amorphous phase is responsible for ferromagnetism in MBE grown $Ge_{1-x}Mn_x$ films. Amorphous $Ge_{1-x}Mn_x$ films, grown by ultra high vacuum thermal coevaporation, also show the presence of embedded nanocrystals [11]. Similarly, high temperature furnace melting techniques produce spatially inhomogeneous samples [17]. For high energy Mn-ion implanted Ge samples [12], Ottaviano *et al*. have reported the presence of ferromagnetic Mn_5Ge_3 nanoparticles [14]. Also for high energy Mn-ion implanted Ge samples [13], transmission electron microscope (TEM) images clearly show presence of two distinct ion-implanted regions in as-implanted samples. These samples also show double hysteresis after annealing, indicating the presence of other phases in annealed samples [13]. For Ref. 15 samples as well, XRD data clearly show the presence of other Ge and Mn ferromagnetic phases. Moreover, none of these Mn-ion implanted studies have conclusively excluded the possibility of defect-induced ferromagnetism as the origin of ferromagnetic behavior [23,24]. As a result, all these previous studies have not been able to clearly answer the following very important basic questions regarding the Mn-doped Ge system: a) What are the magnetic properties of crystalline Mn-doped Ge phase without any second phase? b) What are the magnetic properties of amorphous Mn-doped Ge phase? c) What are the magnetic properties of annealed Mn-ion implanted Ge samples which have no second phase? d) And what is the origin of ferromagnetism in Mn-ion

implanted Ge samples? In this paper we have tried to answer those basic questions by very carefully studying the properties of low energy Mn-ion implanted epitaxial Ge thin films, grown on Si (100) wafers. We have shown that there is no significant second phase of Ge and Mn present in our amorphous samples and while the amorphous Mn-doped Ge phase is ferromagnetic, the annealed crystalline Mn-doped Ge phase is paramagnetic. We have also shown that Mn atoms in amorphous Mn-doped Ge phase have localized magnetic moments and those moments are ferromagnetically coupled with each other below the Curie temperature. Moreover, we report a basic magnetic phase diagram of amorphous Mn-doped Ge. We feel that this approach of Mn-doped epitaxial Ge films on Si wafers is attractive from the point of view that if spintronic devices are going to be used in concert with Si-based nanoelectronics, then there have to be schemes to integrate DMS on Si substrates.

II. EXPERIMENTAL DETAILS

The Ge layers were grown on (100) Si wafers in a custom-built cold wall ultra high vacuum chemical vapor deposition (UHV-CVD) system. A trace amount of C was introduced in Ge during the epitaxial growth process to facilitate 2-D growth of Ge directly on Si surface and also to reduce bulk extended defects in the epitaxial Ge layer [25]. A thin Si buffer layer was also grown on Si prior to Ge growth to improve the interface quality. Disilane (Si_2H_6), methyl-germane (CH_3GeH_3) and germane (GeH_4) gases were used as the Si, C and Ge precursors, respectively. The methyl-germane precursor was a 10% mixture diluted in He, whereas GeH_4 was a 40% mixture with He. The starting substrates were *n*-type Si (100) wafers with resistivities of 1-10 Ω·cm. Before inserting the substrates into the load-lock of the UHV-CVD system, the wafers were cleaned in a piranha solution followed by a 40:1 de-ionized H_2O:HF dip for 40 seconds. The Si wafers were then immediately inserted into the load lock chamber, which was pumped down to below 10^{-6} Torr, before transferring them into the process chamber. The process chamber base pressure before deposition was below 9×10^{-10} Torr. The Ge layers were grown at 450°C at a GeH_4 flow rate of 20 sccm and CH_3GeH_3 flow rate of 0.7 sccm and the gas pressure controlled at 7 mTorr [25].

20 keV energy Mn^+ ions were implanted into 4-inch diameter epitaxial Ge samples with four different doses: a) $1.5\times10^{16}/cm^2$, b) $1.1\times10^{16}/cm^2$, c) $5.5\times10^{15}/cm^2$, d) $2.5\times10^{15}/cm^2$ at 7° tilt angle. These samples so obtained will be denoted as A, B, C and D, respectively. During ion implantation, samples were kept at 300°C

to minimize crystal damage. Under these conditions, the Mn projected range is about 17 nm and the straggle is about 9 nm, as determined by TRIM calculations. Figure 1 is a low-resolution cross-sectional TEM image of sample A, showing Mn-implanted region and epitaxial Ge layer on top of Si (100).

After ion implantation, the samples were cut into 6 mm × 6 mm squares for magnetic property measurements, and 1 cm × 1 cm squares for synchrotron grazing-incident x-ray diffraction (GI-XRD), x-ray absorption spectroscopy (XAS), x-ray photoelectron spectroscopy (XPS), x-ray magnetic circular dichroism (XMCD), and secondary ion mass spectrometry (SIMS) studies, and smaller samples were taken for transmission electron microscopy (TEM) analysis. Teflon tweezers were always used throughout the experiments in order to minimize spurious ferromagnetic impurity incorporation during sample handling [26]. The smaller sample pieces were also cleaned by ultra-sonication in acetone for 2 minutes, followed by isopropyl alcohol (IPA) to remove all surface contaminants. Isochronal (90 seconds) and isothermal (at 300^{o}C) anneals were performed in an N_2 environment to study the structural changes in these ion implanted films.

Dynamic SIMS was used to determine Mn and O profiles for all four samples (Figure 2). Actual total Mn-implant doses were calculated from Mn SIMS profiles and were found to be in good agreement with intended implant doses (values already mentioned). Also from these Mn SIMS profiles of sample A, B, C and D, it was found that approximate peak Mn concentrations in the implanted region are about 16at%, 12at%, 6at%, and 2at%, respectively and average Mn concentrations in the implanted region are $9.3\times10^{21}/cm^3$, $7.5\times10^{21}/cm^3$, $3.0\times10^{21}/cm^3$, and $7.8\times10^{20}/cm^3$, respectively. It can be seen that the peak of the Mn profile for the lowest implant dose agrees with the projected range predicted by TRIM calculation, but there is a slight shift of the peak towards the surface for the higher implant doses for reasons that are not clearly understood. Repeated SIMS measurements confirmed this trend, and could be due to some sputtering of the Ge surface during the Mn implant. However, we must point out that the main conclusions about the ferromagnetic properties of these layers do not depend on the precise Mn peak location, but more on the Mn concentration and total dose, which were confirmed by SIMS measurements. Oxygen SIMS profiles of four samples indicate presence of some oxygen in top 3 nm of our samples. The inset of Figure 2 shows the oxygen SIMS profile of sample A.

III. RESULTS AND DISCUSSION

Magnetic Properties of Mn-implanted epitaxial Ge Thin Films

In-plane temperature dependent magnetic moment measurements were performed at 0.2 Tesla down to 5 K, using a superconducting quantum interference device (SQUID) magnetometer (Figure 3). Each magnetization curve is made up of magnetic field-cooled and zero-field-cooled data and a spin-glass phase was observed at very low temperatures. It was found that temperature dependent field-cooled and zero-field-cooled magnetic moments diverge below a certain temperature, which is defined as the spin-glass temperature. A spin-glass phase is expected because at these high Mn concentrations, many defects are present as well as possibly binary phases of Ge and Mn [27,28]. Curie temperatures are estimated from these temperature-dependent magnetic moment measurements and it is defined as the temperature at which magnetic moment goes to zero. Temperature-dependent magnetization (Figure 3) and magnetic hysteresis measurements (Figure 4) show that the first three samples are ferromagnetic and the fourth sample is paramagnetic. Moreover, Curie temperatures (170 K, 145 K, 130 K, respectively) and saturated magnetization (20.0 emu/cm^3, 9.5 emu/cm^3, 5.9 emu/cm^3, respectively) of the three ferromagnetic samples scale monotonically with total Mn-implant dose, as shown in the inset of Figure 3. Temperature-dependent magnetic hysteresis shows that the coercive field is non-zero only below a certain temperature, which is also known as the superparamagnetic temperature. Above this superparamagnetic temperature, the coercive field is very small and hysteresis is S-shaped, as shown in the inset of Figure 4. For sample A, superparamagnetic temperature is about 20 K. Figure 5 shows the dependence of the Curie temperature, spin-glass temperature and superparamagnetic temperature as a function of Mn-implant dose for our 4 samples.

Structural Characterization of Mn-implanted epitaxial Ge Thin Films

In order to better understand the origin of the ferromagnetism in Mn-implanted epitaxial Ge (Ge:Mn) thin films, high resolution transmission electron microscopy (HR-TEM), XPS and GI-XRD studies were performed. Cross-sectional HR-TEM images of as-implanted samples indicate that the ion-implanted region is amorphous, without any precipitation, above the end of implant range (Figure 6(a)). The XPS spectra (data not shown) indicate the presence of oxygen in the top 3 nm of the as-implanted samples; both Ge and Mn in the top 3 nm are partially oxidized. This result agrees well with oxygen SIMS profiles. Moreover, below top 3 nm, XPS

spectra of both Ge and Mn of our as-implanted Mn-doped Ge samples are indistinguishable from their respective pure elemental XPS spectra.

Synchrotron GI-XRD experiments were performed on sample A at Stanford Synchrotron Radiation Lightsource (SSRL) beamline 2-1 at 10 keV x-ray energy (Figure 7). For a 10 keV photon source and incident angles of 0.10^o, 0.15^o and 0.20^o, the estimated x-ray penetration depths for $Ge_{0.84}Mn_{0.16}$ are about 2.4 nm, 2.8 nm and 3.6 nm, respectively. For very low incident angles (0.10^o and 0.15^o), GI-XRD data show the presence of (110) GeO_2 and (102) MnO_2 peaks. These two oxide phases have also been observed in TEM and XPS studies on the surface of implanted region. For higher incidence angle of 0.20^o, XRD data shows the presence of (111), (222) and other higher order Ge peaks, all of which are very broad. Moreover, there is also a very weak and broad XRD peak that matches with the strongest peak of many known binary alloys of Ge and Mn (for example Ge_2Mn_5, Mn_2Ge, GeMn, $GeMn_3$, Ge_8Mn_{11} and Ge_3Mn_5). But the concentrations of these phases are very low compared to the amorphous Ge:Mn phase, as indicated by the predominant Ge diffraction peaks. However, very broad Ge diffraction peaks for all three incident angles indicate that there is no long-range order in the Mn-implanted Ge region, as has also been observed by HR-TEM studies.

Annealing experiments were performed to monitor the evolution of Ge:Mn microstructure and its relation to magnetization and Curie temperature. Isothermal annealing of sample A at 300^oC shows that as the annealing time increases, saturation magnetization decreases, but Curie temperature remains the same, as shown in Figure 8. Moreover, the normalized temperature-dependent magnetization plots of as-implanted and annealed (for different times) samples superimpose on each other (Figure 8 (inset)). These results suggest that the phase, which is responsible for ferromagnetism in Ge:Mn, is not changing but its amount (per unit sample volume) decreases with increasing isothermal annealing time. Furthermore, the sample annealed at 600^oC for 90 seconds recrystallizes completely and becomes paramagnetic. Figure 6 shows high resolution TEM and high resolution scanning transmission electron microscopy (HRSTEM) cross sections of an as-implanted film and one annealed at 600^oC for 90 seconds. It is clear from these cross-sectional TEM images that the as-implanted film shows an amorphous region above the end of implant range; whereas the annealed film shows a completely recrystallized implanted region as well as a thin region at the top of the film that contains oxygen as determined by photoemission electron microscopy (PEEM), data not shown. Therefore it seems that ferromagnetism is associated with the presence of an amorphous phase, rather than a crystalline phase. It is not associated with the

presence of crystalline Ge_3Mn_5 or other ferromagnetic Ge and Mn alloys. A similar effect has also been observed by Sugahara *et al.* [9], where they intentionally grew an amorphous layer of Mn-doped Ge by MBE on SiO_2.

Synchrotron X-ray Studies of Mn-implanted Epitaxial Ge Thin Film

To further address the magnetism of the Mn sites, we performed XAS and XMCD measurements at beamline 6.3.1 at the Advanced Light Source (ALS) in Berkeley, CA and beamline 13-1 at the Stanford Synchrotron Radiation Lightsource (SSRL). Both beamlines provide circularly polarized soft x-rays in the range between 500 eV and 1500 eV. XAS and XMCD allow for studies of the magnetic properties of each element in a complex heterogeneous sample. Incoming x-ray photon initiates a transition of a core level electron, in this case Mn 2*p*, into an empty final state above the Fermi level, here the 3*d* levels. Since the photon energy at which such a transition occurs is specific for each element, one can probe the empty density-of-states (DOS) in an element-specific manner. Furthermore, by using circularly polarized x-rays only electrons with a particular spin are excited, which allows for a spin sensitive investigation of the empty DOS. In our setup, the x-ray absorption cross section is detected by monitoring the secondary electron yield while scanning the photon energy across the desired energy range in discrete steps. The sample is mounted between the yokes of an electromagnet so that the magnetization of the sample can be reversed for each data point. Two x-ray absorption spectra are obtained in this way, one with the sample magnetization parallel to the helicity of the incoming circularly polarized x-rays and one with the magnetization antiparallel to it. The difference between these two spectra is then referred to as XMCD spectrum and contains information about the magnetic moment of the particular atomic species [29,30].

There are several XAS and XMCD studies on Mn-doped Ge epitaxial films [31-33]. However the possible presence of secondary phases, including oxides, makes it typically difficult to figure out the intrinsic magnetic moments of Mn in amorphous phase from those studies. We have therefore taken extra precautions in order to minimize the effects of oxidation on our spectroscopy results. A small 1 inch square of sample A was loaded in a high vacuum chamber (with base pressure less than 10^{-9} Torr) and then about 5 nm top layers were etched by 200 keV Ar-ion sputtering, immediately followed by *in situ* 2 nm Ta deposition to stop further oxidation. Figure 9 shows room temperature experimental Mn 2*p* XAS spectrum of Ta-capped sample A, calculated Mn^{2+} and Mn^{3+} spectra in spherical symmetry and calculated Mn^{2+} spectrum in tetragonal symmetry. These spectra are calculated using CTM4XAS charge transfer multiplet program [34]. The experimental Mn 2*p* XAS spectrum is

very similar to calculated Mn^{2+} XAS spectrum in spherical symmetry, but very different from other two calculated spectra. This indicates that there exists almost no long-range crystalline order and Mn atoms of amorphous $Ge_{1-x}Mn_x$ are isolated double donors with localized magnetic moments of 2.5 Bohr magnetons per Mn atom. In comparison, the average magnetic moment measured by the SQUID magnetometer is only 0.23 Bohr magnetons per Mn atom for sample A. This clearly indicates that only a fraction of Mn atoms (about 10%) are ferromagnetically coupled with each other. This is expected for an ion-implanted sample, which has a near Gaussian distribution of Mn concentration, as evident from the SIMS profile (Fig. 2). We think that Mn atoms at the tail of this distribution are not ferromagnetically coupled to each other, thus giving a lower than expected magnetization.

To address the temperature dependence of the magnetization in our samples, we measured XMCD spectra of sample A at different temperatures between 15K and 150K, as well as at room temperature. Since our detection method is surface sensitive, we performed our experiments on two different samples. One sample is referred to the as-implanted sample, while the surface of the etched sample was prepared by etching the top 5 nm. In the etched sample, the implantation layer is closer to the surface, thus yielding more information about deeper implantation layers. The Mn XMCD spectrum for the as-implanted sample obtained at 15 K is shown in the inset of Figure 10, while the temperature dependence of the peak value of the Mn XMCD spectrum at the L_3 resonance just below 640eV is shown in Figure 10. The maximum peak value of the XMCD spectrum can be used as a quantitative measure of how the Mn magnetization changes with temperature as long as the coordination around the Mn does not change with temperature [35]. For both samples the Mn XMCD decreases upon increasing the temperature and reaches a constant value at about 150 K. This remaining XMCD contribution does not change significantly above 150 K and can be attributed to the paramagnetic phase, while the increase in XMCD below 150 K is linked to the appearance of ferromagnetic order, as previously discussed. The etched sample consistently shows a larger XMCD signal, since the effective Mn concentration observed in this sample is higher. Other than the increased XMCD signal, we do not find any differences in the x-ray absorption spectrum or XMCD spectrum between the two samples. The shape of the XMCD spectrum, as shown in the inset of Figure 10, is typical for localized Mn moments [36] and does not depend on the preparation method of the surface. Altogether, the x-ray absorption spectra of Mn-doped Ge indicate that the Mn moments order ferromagnetically below 150 K and therefore this is not a defect-induced magnetic ordering [23,24]. In comparison, the previous XMCD study on MBE grown epitaxial $Ge_{1-x}Mn_x$ does not show any remnant XMCD signal [32].

IV. CONCLUSION

We have studied ferromagnetism in Mn-implanted epitaxially grown Ge on Si (100) wafer. GI-XRD data and TEM images show that Mn-implanted Ge thin films are amorphous, without any significant second phase. We suggest that this amorphous phase is responsible for ferromagnetism. XMCD data show that localized Mn moments in the amorphous region are ferromagnetically coupled with each other below Curie temperature. Curie temperature and saturated magnetic moment are monotonic function of Mn implant dose above 6at%. Isothermal annealing of Ge:Mn films at 300^{o}C for up to 1200 seconds decreases the saturated magnetization but does not change the Curie temperature, suggesting that the volume of magnetic phase slowly decreases with annealing time at 300^{o}C. This is also supported by the fact that high temperature annealing causes recrystallization and transforms the material into a paramagnet. These results shed light on other studies of Mn-doped Ge systems, in that we have identified the amorphous phase as a possible source of ferromagnetism in these materials.

ACKNOWLEDGMENTS

This work was supported by SWAN-NRI, NSF DMR 0605828, and Welch Foundation F-1191. SSRL and ALS are national user facilities supported by the Department of Energy, Office of Basic Energy Sciences. SSRL is operated by Stanford University and ALS is operated by the University of California under contract No. DE-AC02-05CH11231.

REFERENCES

[1] T. Jungwrith, J. Sinova, J. Masek, J. Kucěra, and A. H. MacDonald, "Theory of ferromagnetic (III,Mn)V semiconductors", Reviews of Modern Physics **78**, 809 (2006).

[2] A. J. R. de Silva, A. Fazzio, and A. Antonelli, "Stabilization of substitutional Mn in silicon-based semiconductors", Physical Review B **70**, 193205 (2004).

[3] W. Zhu, Z. Zhang, and E. Kaxiras, "Dopant-Assisted Concentration Enhancement of Substitutional Mn in Si and Ge", Physical Review Letters **100**, 027205 (2008).

[4] H. Chen, W. Zhu, E. Kaxiras, and Z. Zhang, "Optimization of Mn doping in group-IV-based dilute magnetic semiconductors by electronic codopants", Physical Review B **79**, 235202 (2009).

[5] A. Continenza and G. Profeta, "Mn doping in model amorphous Si and Ge: a theoretical investigation", Journal of Physics: Conference Series **200**, 032014 (2010).

[6] Y. D. Park, A. T. Hanbicki, S. C. Erwin, C. S. Hellberg, J. M. Sullivan, J. E. Mattson, T. F. Ambrose, A. Wilson, G. Spanos, and B. T. Jonker, "A group-IV ferromagnetic semiconductor: $Ge_{1-x}Mn_x$", Science **295**, 651 (2002).

[7] A. P. Li, J. Shen, J. R. Thompson, and H. H. Weitering, "Ferromagnetic percolation in Mn_xGe_{1-x} dilute magnetic semiconductor", Applied Physics Letters **86**, 152507 (2005).

[8] N. Pinto, L. Morresi, M. Ficcadenti, R. Murri, F. D'Orazio, F. Lucari, L. Boarino, and G. Amato, "Magnetic and electronic transport percolation in epitaxial $Ge_{1-x}Mn_x$ films", Physical Review B **72**, 165203 (2005).

[9] S. Sugahara, K. L. Lee, S. Yada, and M. Tanaka, "Precipitation of Amorphous Ferromagnetic Semiconductor Phase in Epitaxially Grown Mn-Doped Ge Thin Films", Japanese Journal of Applied Physics **44,** L1426-L1429 (2005).

[10] P. De Padova, J.-P. Ayoub, I. Berbezier, J.-M. Mariot, A. Taleb-Ibrahimi, M.C. Richter, O. Heckmann, A.M. Testa, D. Fiorani, B. Olivieri, S. Picozzi and K. Hricovini, "Mn_xGe_{1-x} thin layers studied by TEM, X-ray absorption spectroscopy and SQUID magnetometry", Surface Science **601**, 2628 (2007).

[11] J. Deng, Y. Tian, S. Yan, Q. Cao, G. Liu, Y. Chen, L. Mei, G. Ji and Z. Zhang, "Magnetism of amorphous $Ge_{1-x}Mn_x$ magnetic semiconductor films", Journal of Applied Physics **104**, 013905 (2008).

[12] M. Passacantando, L. Ottaviano, F. D'Orazio, F. Lucari, M. De Biase, G. Impellizzeri and F. Priolo, "Growth of ferromagnetic nanoparticles in a dilute magnetic semiconductor obtained by Mn^+ implantation on Ge single crystals", Physicsl Review B **73**, 195207 (2006).

[13] A. Verna, L. Ottaviano, M. Passacantando, S. Santucci, P. Picozzi, F. D'Orazio, F. Lucari, M. De Biase, R. Gunnella, M. Berti, A. Gasparotto, G. Impellizzeri and F. Priolo, "Ferromagnetism in ion implanted amorphous and nanocrystalline Mn_xGe_{1-x}", Physical Review B **74**, 085204 (2006).

[14] L. Ottaviano, M. Passacantando, S. Picozzi, A. Continenza, R. Gunnella, A. Verna, G. Bihlmayer, G. Impellizzeri and F. Priolo, "Phase separation and dilution in implanted Mn_xGe_{1-x} alloys", Applied Physics Letters **88**, 061907 (2006).

[15] J. Chen, K. L. Wang and K. Galatsis, "Electrical field control magnetic phase transition in nanostructured Mn_xGe_{1-x}", Applied Physics Letters **90**, 012501 (2007).

[16] S. Cho, S. Choi, S. C. Hong, Y. Kim, J. B. Ketterson, B.-J. Kim, Y. C. Kim, and J.-H. Jung, "Ferromagnetism in Mn-doped Ge", Physical Review B **66**, 033303 (2002).

[17] J.-S. Kang, G. Kim, S. C. Wi, S. S. Lee, S. Choi, S. Cho, S. W. Han, K. H. Kim, H. J. Song, H. J. Shin, A. Sekiyama, S. Kasai, S. Suga and B. I. Min, "Spatial Chemical Inhomogeneity and Local Electronic Structure of Mn-Doped Ferromagnetic Semiconductors", Physical Review Letters **94**, 147202 (2005).

[18] E. Biegger, L. Stäheli, M. Fonin, U. Rüdiger and Y. S. Dedkov, "Intrinsic ferromagnetism versus phase segregation in Mn-doped Ge", Journal of Applied Physics **101**, 103912 (2007).

[19] O. Kazakova, J. S. Kulkarni, J. D. Holmes, and S. O. Demokritov, "Room-temperature ferromagnetism in $Ge_{1-x}Mn_x$ nanowires", Physical Review B (Condensed Matter and Materials Physics) **72,** 094415 (2005).

[20] Y. J. Cho, C. H. Kim, H. S. Kim, W. S. Lee, S.-H. Park, J. Park, S. Y. Bae, B. Kim, H. Lee and J.-Y. Kim, "Ferromagnetic $Ge_{1-x}M_x$ (M=Mn, Fe, and Co) Nanowires", Chemistry of Materials **20**, 4694 (2008).

[21] M. Jamet, A. Barski, T. Devillers, V. Poydenot, R. Dujardin, P. Bayle-Guillemaud, J. Rothman, E. Bellet-Amalric, A. Marty, J. Cibert, R. Mattana, and S. Tatarenko, "High-Curie-temperature ferromagnetism in self-organized $Ge_{1-x}Mn_x$ nanocolumns", Nature Materials **5**, 653 (2006).

[22] F. Xiu, Y. Wang, J. Kim, A. Hong, J. Tang, A. P. Jacob, J. Zou and K. L. Wang, "Electric-field-controlled ferromagnetism in high-Curie-temperature $Mn_{0.05}Ge_{0.95}$ quantum dots", Nature Materials **9**, 337 (2010).

[23] J.M.D. Coey, "Dilute Magnetic Oxides", Current Opinion in Solid State and Materials Science **10**, 83 (2006).

[24] M. Khalid, M. Ziese, A. Setzer, P. Esquinazi, M. Lorenz, H. Hochmuth, M. Grundmann, D. Spemann, T. Butz, G. Brauer, W. Anwand, G. Fischer, W. A. Adeagbo, W. Hergert, and A. Ernst, "Defect-induced magnetic order in pure ZnO films", Physical Review B **80**, 035331 (2009).

[25] D. Q. Kelly, J. P. Donnelly, S. Dey, S. V. Joshi, D. I. G. Gutiérrez, M. J. Yacamán, and S. K. Banerjee, "BC high-κ/metal gate Ge/C alloy pMOSFETs fabricated directly on Si (100) substrates", IEEE Electron Device Letters **27**, 265 (2006).

[26] D. W. Abraham, M. M. Frank and S. Guha, "Absence of magnetism in hafnium oxide films", Applied Physics Letters **87**, 252502 (2005).

[27] C. Jaeger, C. Bihler, T. Vallaitis, S. T. B. Goennenwein, M. Opel, R. Gross and M. S. Brandt, "Spin-glass-like behavior of Ge:Mn", Physical Review B **74**, 045330 (2006).

[28] S. H. Song, M. H. Jung, and S. H. Lim, "Spin glass behaviour of amorphous Ge-Mn alloy thin films", Journal of Physics: Condensed Matter **19**, 036211 (2007).

[29] B. T. Thole, P. Carra, F. Sette, and G. van der Laan, "X-ray circular dichroism as a probe of orbital magnetization", Physical Review Letters **68**, 1943 (1992).

[30] B. T. Thole and G. van der Laan, "Sum rules for magnetic dichroism in rare earth 4*f* photoemission", Physical Review Letters **70**, 2499 (1993).

[31] S. Picozzi, L. Ottaviano, M. Passacantando, G. Profeta, A. Continenza, F. Priolo, M. Kim and A. J. Freeman, "X-ray absorption spectroscopy in Mn_xGe_{1-x} dilute magnetic semiconductor: Experiment and theory", Applied Physics Letters **86**, 062501 (2005).

[32] P. Gambardella, L. Claude, S. Rusponi, K. J. Franke, H. Brune, J. Raabe, F. Nolting, P. Bencok, A. T. Hanbicki, B. T. Jonker, C. Grazioli, M. Veronesa, and C. Carbone, "Surface characterization of Mn_xGe_{1-x} and $Cr_yMn_xGe_{1-x-y}$ dilute magnetic semiconductors", Physical Review B **75**, 125211 (2007).

[33] S. Ahlers, P. R. Stone, N. Sircar, E. Arenholz, O. D. Dubon, and D. Bougeard, "Comparison of the magnetic properties of GeMn thin films through Mn *L*-edge x-ray absorption", Applied Physics Letters **95**, 151911 (2009).

[34] Eli Stavitski and Frank M.F. de Groot, "The CTM4XAS program for EELS and XAS spectral shape analysis of transition metal *L* edges", Micron **41**, 687 (2010).

[35] H. Ohldag, V. Solinus, F. U. Hillebrecht, J. B. Goedkoop, M. Finazzi, F. Matsukura and H. Ohno, "Magnetic moment of Mn in the ferromagnetic semiconductor ($Ga_{0.98}Mn_{0.02}$)As", Applied Physics Letters **76**, 2928 (2000).

[36] L. Zeng, E. Helgren, M. Rahimi, F. Hellman, R. Islam, B. J. Wilkens, R. J. Culbertson, and D. J. Smith, "Quenched magnetic moment in Mn-doped amorphous Si films", Physical Review B **77**, 073306 (2008).

Table 1: This table summarizes Mn-implant dose, Mn concentration, and magnetic properties of four ion implanted samples.

Figure 1: Low resolution TEM image of as-implanted sample A, showing Mn-implanted region and epitaxially grown Ge on top of Si (100) wafer.

Figure 2: Manganese concentration SIMS profiles of four as-implanted Ge:Mn samples. The inset plot shows oxygen SIMS profile of sample A.

Figure 3: Temperature dependent in-plane saturated magnetization (at 0.2 Tesla) plot for four Mn-implanted epitaxial Ge samples. Each magnetization curve is made up of magnetic zero-field-cooled and field-cooled data. The inset plot shows that measured Curie temperatures and saturated magnetizations of Mn-implanted Ge samples scale monotonically with Mn implant dose.

Figure 4: Magnetic hysteresis of four Mn-doped Ge samples at 10 K. The inset shows magnetic hysteresis of sample A at 50 K.

Figure 5: This basic phase diagram shows the dependence of Curie temperature, spin glass temperature and superparamagnetic temperature on total Mn-implant dose.

Figure 6. Cross-sectional TEM images of (a) as-implanted sample A, showing amorphous implanted region and crystalline Ge underlayer, with (b) a HRSTEM image of the same region indicating the higher atomic number of the implanted region with respect to the substrate; (c) the same sample annealed at 600ºC for 90s, showing a fully recrystallized region of Ge:Mn with a thin layer of a well order phase of GeMnO at the top of the film shown in (d).

Figure 7: Synchrotron GI-XRD plot of sample A. (*This weak broad peak matches with highest peak of several Ge & Mn alloys: Ge_2Mn_5, Mn_2Ge, GeMn, $GeMn_3$, Ge_8Mn_{11} and Ge_3Mn_5.)

Figure 8: Temperature dependent in-plane saturated magnetization of sample A before and after annealing at 300^oC for different durations. The inset shows normalized temperature-dependent magnetization plots for as-implanted and annealed (for different times) sample A.

Figure 9: Room temperature experimental Mn 2*p* XAS spectrum of Ta-capped sample A, calculated Mn^{2+} and Mn^{3+} spectra in spherical symmetry and calculated Mn^{2+} spectrum in tetragonal symmetry. These spectra are calculated using CTM4XAS charge transfer multiplet program [34].

Figure 10: Normalized Mn XMCD of the as-implanted and etched sample A obtained in saturation by applying a magnetic field of ±1.8 Tesla. In both cases the Mn XMCD remains constant above around 150 K. The inset shows the XMCD spectrum obtained from the as-implanted sample A at 15 K.

Table 1

Sample	Implanted Mn Dose	Peak Mn Concen-tration	Average Mn Concen-tration	Magnetic Property	Curie Temp.	Saturated Magnetization (at 5 K, 0.2 T)	Superpara-magnetic Temp.	Spinglass Temperature (at 0.2 Tesla)
	cm^{-2}	at% (approx.)	cm^{-3}		K	emu/cm^3	K	K
A	1.5×10^{16}	16	9.3×10^{21}	Ferro	170	20.0	20	15
B	1.1×10^{16}	12	7.5×10^{21}	Ferro	145	9.5	16	12
C	5.5×10^{15}	6	3.0×10^{21}	Ferro	130	5.9	14	8
D	2.5×10^{15}	2	7.8×10^{20}	Para (up to 5 K)	-	-	-	Not observed (up to 5 K)

Figure 1

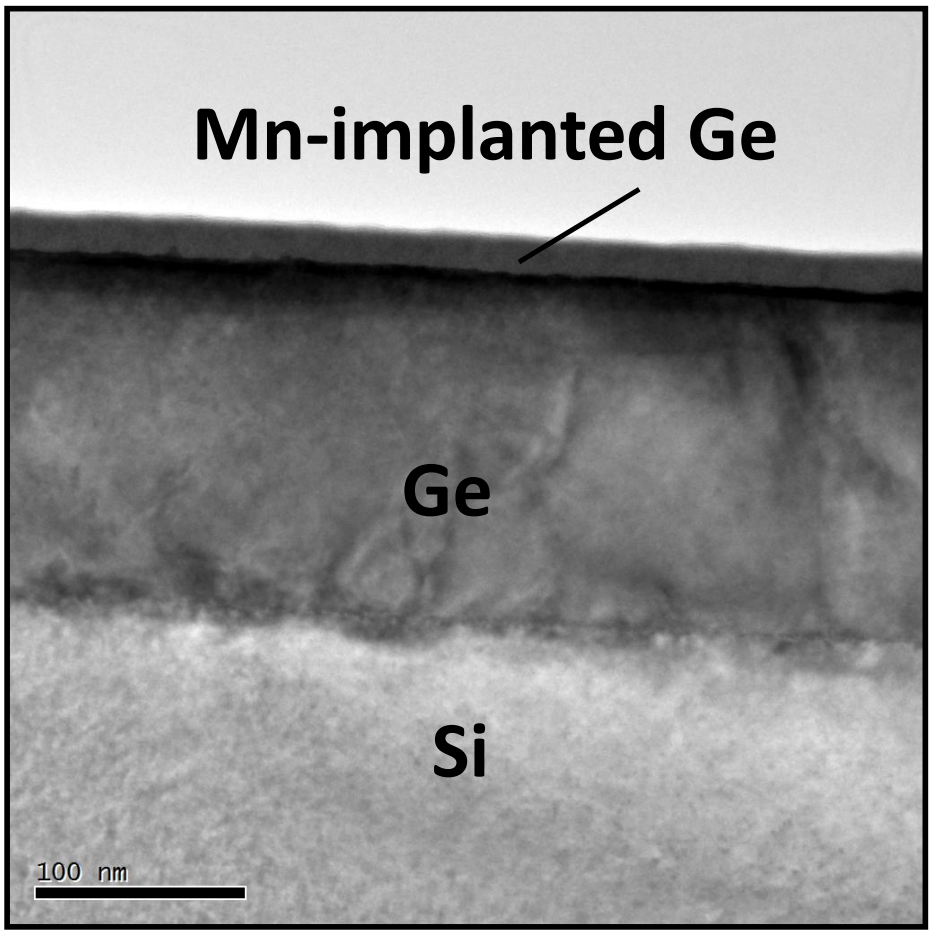

Figure 2

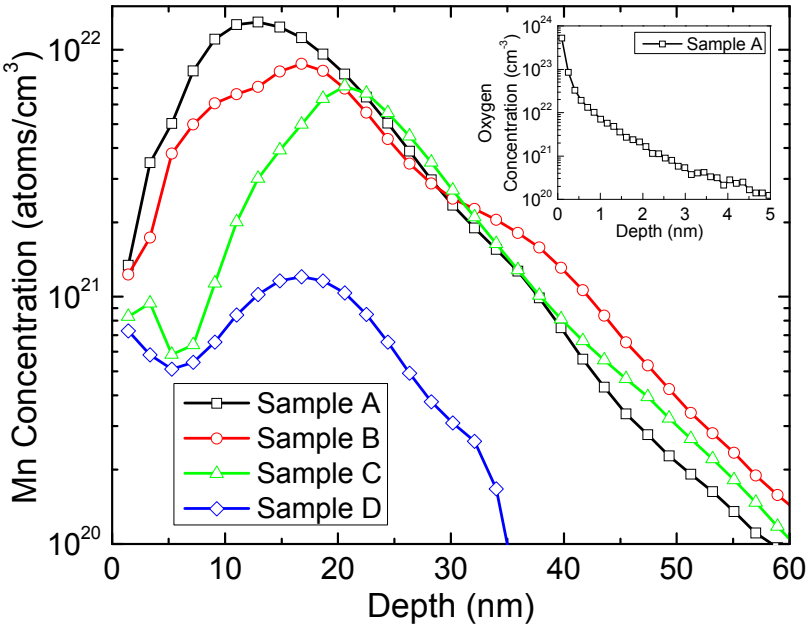
Mn Concentration (atoms/cm^3)
10^{22}
10^{21}
10^{20}
0
10
20
30
40
50
60
Depth (nm)
Sample A
Sample B
Sample C
Sample D
Oxygen Concentration (cm^{-3})
10^{24}
10^{23}
10^{22}
10^{21}
10^{20}
0
1
2
3
4
5
Depth (nm)
Sample A

Figure 3

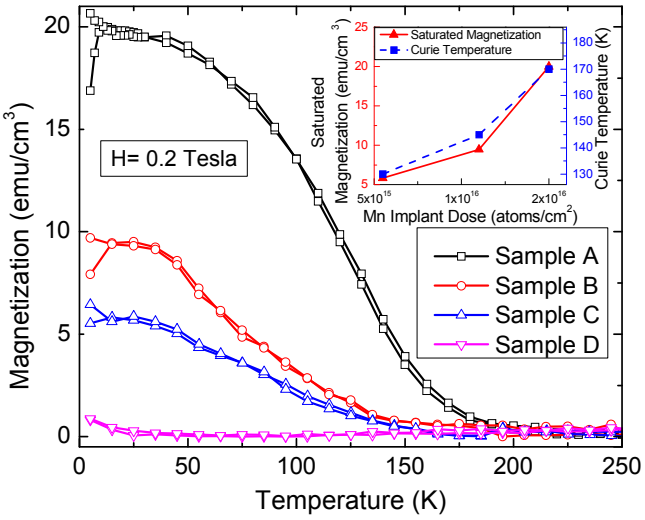
Magnetization (emu/cm^3)
Temperature (K)
H= 0.2 Tesla
Sample A
Sample B
Sample C
Sample D
Saturated Magnetization
Curie Temperature
Saturated Magnetization (emu/cm^3)
Curie Temperature (K)
Mn Implant Dose (atoms/cm^2)

Figure 4

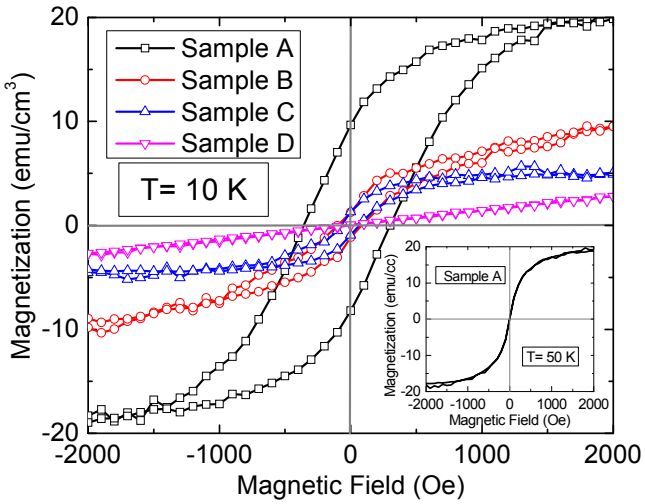
Sample A
Sample B
Sample C
Sample D
T= 10 K
Magnetization (emu/cm3)
Magnetic Field (Oe)
20
10
0
-10
-20
-2000
-1000
0
1000
2000
Sample A
T= 50 K
Magnetization (emu/cc)
Magnetic Field (Oe)

Figure 5

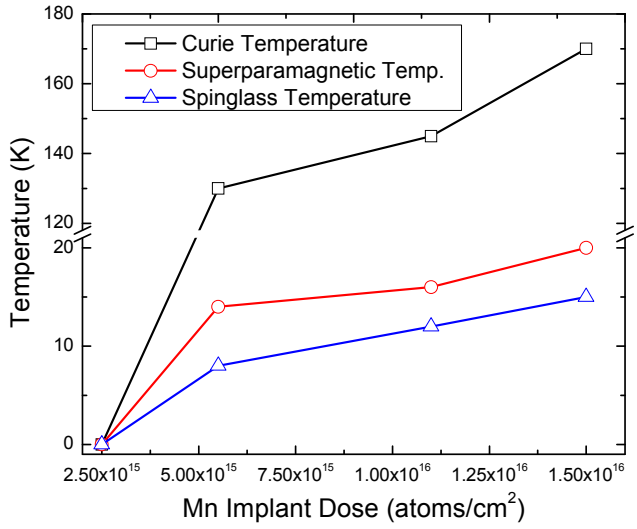
Curie Temperature
Superparamagnetic Temp.
Spinglass Temperature
Temperature (K)
180
160
140
120
20
10
0
2.50x10^15
5.00x10^15
7.50x10^15
1.00x10^16
1.25x10^16
1.50x10^16
Mn Implant Dose (atoms/cm^2)

Figure 6

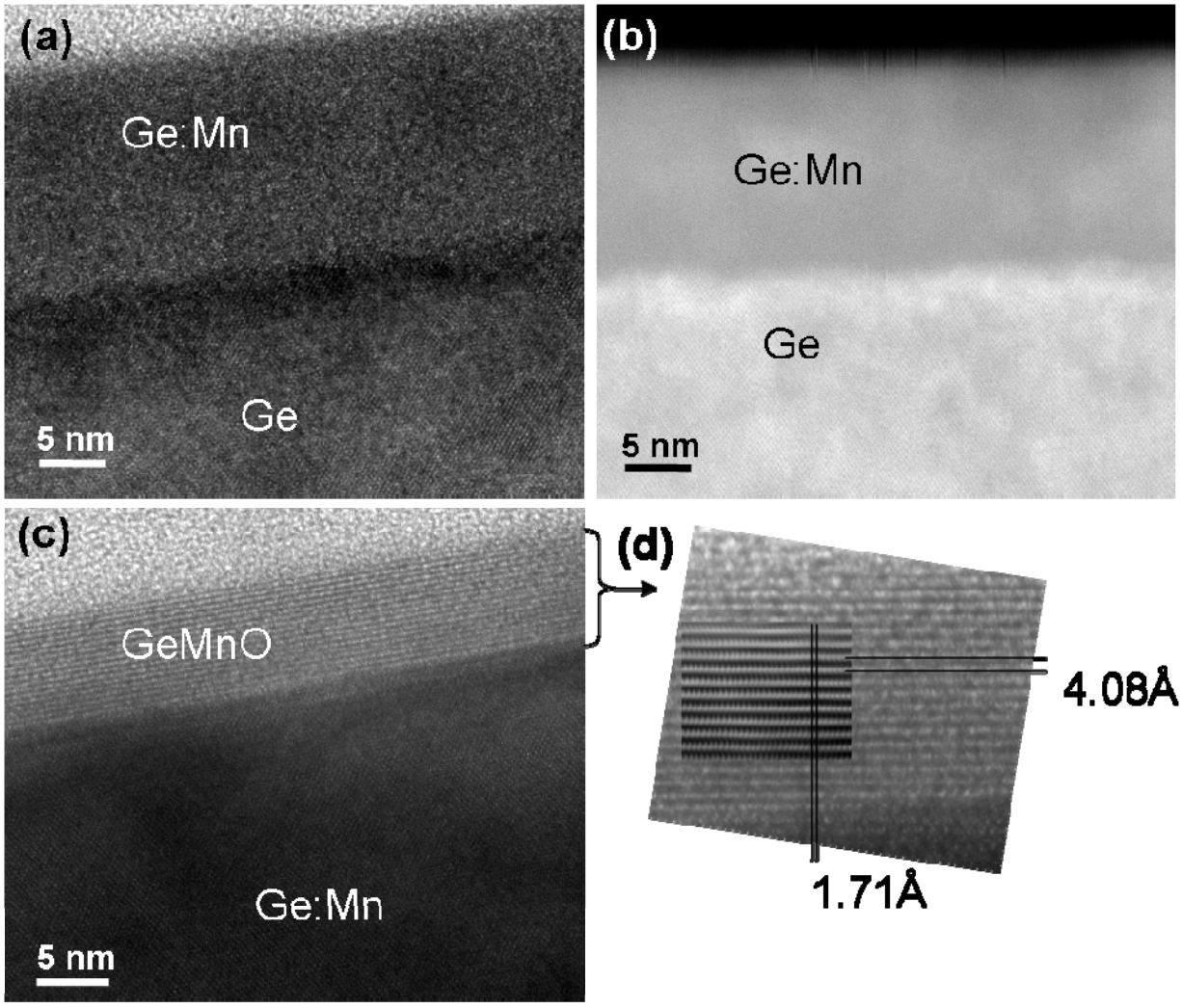

Figure 7

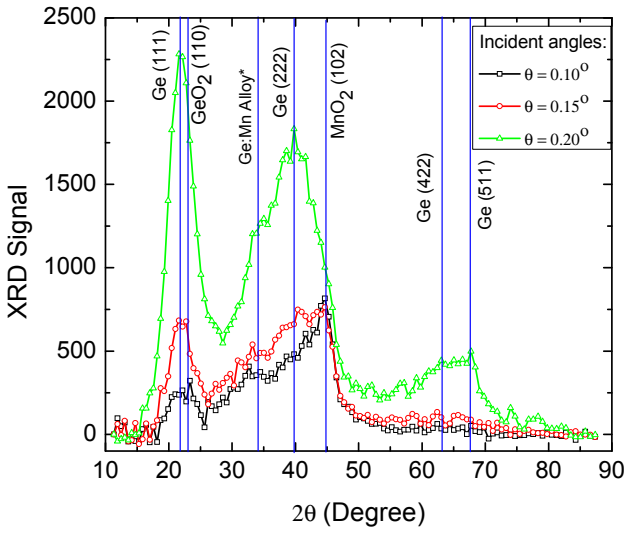
XRD Signal
2θ (Degree)
Incident angles:
θ = 0.10°
θ = 0.15°
θ = 0.20°
Ge (111)
GeO2 (110)
Ge:Mn Alloy*
Ge (222)
MnO2 (102)
Ge (422)
Ge (511)

Figure 8

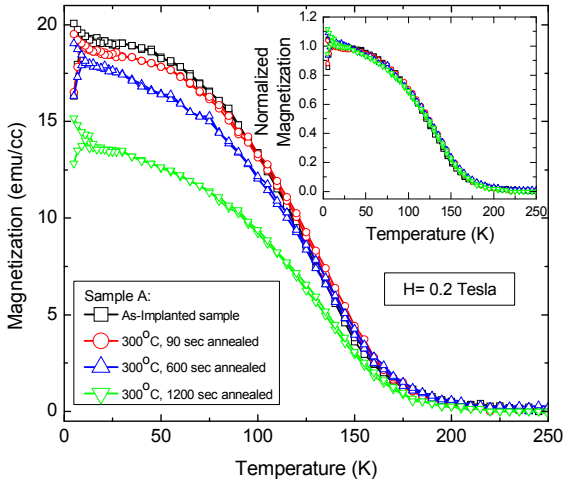
Magnetization (emu/cc)
Temperature (K)
Normalized Magnetization
Temperature (K)
Sample A:
As-Implanted sample
300°C, 90 sec annealed
300°C, 600 sec annealed
300°C, 1200 sec annealed
H= 0.2 Tesla

Figure 9

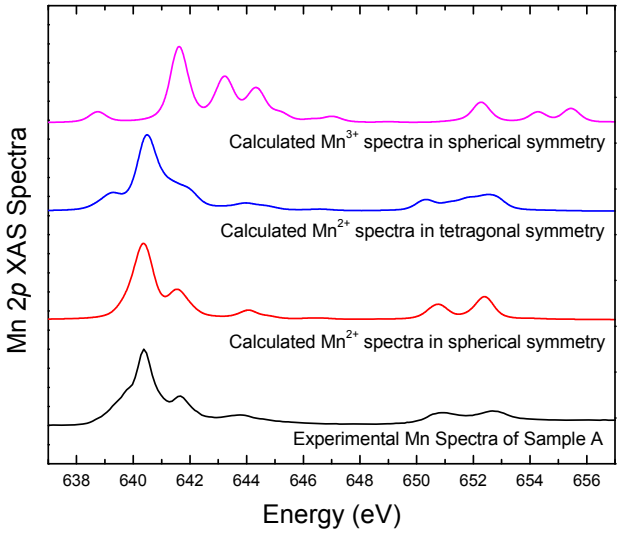
Mn 2p XAS Spectra
Calculated Mn3+ spectra in spherical symmetry
Calculated Mn2+ spectra in tetragonal symmetry
Calculated Mn2+ spectra in spherical symmetry
Experimental Mn Spectra of Sample A
638
640
642
644
646
648
650
652
654
656
Energy (eV)

Figure 10

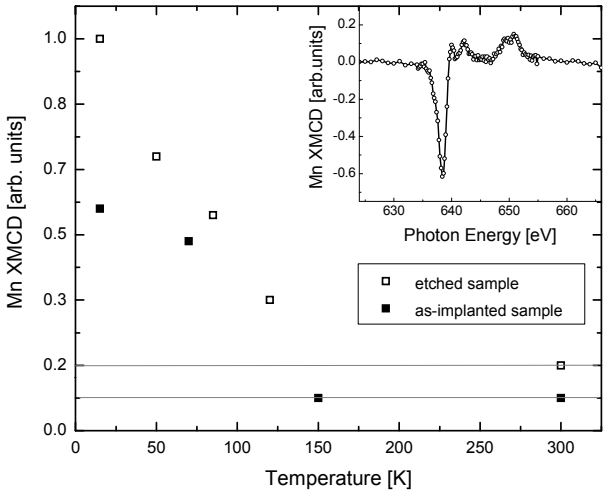
Mn XMCD [arb. units]
Temperature [K]
Mn XMCD [arb.units]
Photon Energy [eV]
etched sample
as-implanted sample